# Pore size analyses of cement paste exposed to external sulfate attack and delayed ettringite formation

Yushan Gu, Renaud Pierre Martin, Othman Omikrine Metalssi, Teddy Fen Chong, Patrick Dangla

# Pore size analyses of cement paste exposed to external sulfate attack and delayed ettringite formation

Yushan GU[a], Renaud-Pierre MARTIN[b], Othman OMIKRINE METALSSI[a], Teddy FEN-CHONG[a], Patrick DANGLA[c,*]

[a] *Université Paris-Est, MAST, FM2D, IFSTTAR, F-77447 Marne-la-Valle, France*
[b] *Université Paris-Est, MAST, EMGCU, IFSTTAR, F-77447 Marne-la-Valle, France*
[c] *Université Paris-Est, Laboratoire Navier (UMR 8205), CNRS, Ecole des Ponts ParisTech, IFSTTAR, F-77455 Marne-la-Vallée, France*

**Abstract**

Experimental studies on cement paste exposed to external sulfate attack (ESA), delayed ettringite formation (DEF), and the coupling effect of both reactions are presented in this paper. The objective is to compare the degraded state of specimens, the length and mass variations, and the pore size distribution (PSD) obtained by mercury intrusion porosimetry (MIP) of cement paste submitted to these different exposure conditions. By comparing the PSD of specimens before and after the sulfate attacks, a global expansion mechanism is proposed: ettringite first precipitates in the biggest pores without inducing obvious expansion, and then penetrates into capillary and gel pores leading to an accelerated swelling. In addition, the coupling effect of ESA and DEF is found to be the most damaging expansion, which raises a high durability problem for cement-based materials.

*Keywords:* Sulfate attacks, ESA, DEF, Coupling effect of ESA and DEF, cement pastes, pore size distribution, ettringite formation.

*Corresponding author
*Email addresses:* yushanjoanna@hotmail.com (Yushan GU), renaud-pierre.martin@ifsttar.fr (Renaud-Pierre MARTIN), othman.omikrine-metalssi@ifsttar.fr (Othman OMIKRINE METALSSI), teddy.fen-chong@ifsttar.fr (Teddy FEN-CHONG), patrick.dangla@ifsttar.fr (Patrick DANGLA)

## 1. Introduction

Sulfate ions, commonly present in sulfate-containing environments (marine environment or groundwater) or construction materials, are critical agents in the engineering field. The origin of sulfate ions leads to a distinction between External Sulfate Attack (ESA) and Internal Sulfate Attack (ISA). Delayed Ettringite Formation (DEF), as a form of ISA, is observed in cementitious materials which experienced elevated temperatures during curing, either from a heating treatment or from an internal high temperature due to the heat released by hydration in massive concrete.

Separate studies intending to understand the damage mechanisms of ESA and DEF have been reported in the literature. In the case of ESA, ettringite precipitates from sodium sulfate solution, forming three distinct zones [1]: a cracked and deteriorated surface zone, followed by a zone of ettringite deposited in the paste, and an interiorly cracked zone which is chemically unaltered. A tensile force is created in the last zone due to the formation of expansive products in the second zone, which leads to cracks in the interior of the mortar. In the former two degraded zones, ettringite is supposed to be formed in large pores which does not lead to an expansion, and then precipitated in smaller pores which contributes to expansions, until all the free aluminates are consumed [2]. Then, the sulfate concentration increases to a critical level which provides a driving force for the precipitation of ettringite crystals in small pores within the C-S-H. The onset of the expansion starts when the material cannot resist the pressure resulting from the interaction between the ettringite and the surrounding matrix of cement paste, namely the crystallization pressure [2, 3]. The mechanism proposed in [1] is influenced by surface leaching in a limited way since the external solution (with a pH lower than the one of the cementitious material) is not renewed during the test [4]. In the field, the surface leaching due to the external low pH condition is much higher and has a significant influence on the degradation process. In the case of DEF, a high temperature above about 65 °C can decompose the primary ettringite in hydrated calcium monosulphoa-

luminate, releasing sulfates to the pore solution [5, 6, 7]. Part of sulfate and aluminate ions may be adsorbed on C-S-H [8, 9], which will be released later to trigger ettringite crystallization at ambient temperature. Therefore, the ettringite is postulated to initially occur in C-S-H gel and then in cracks and voids [8]. Ettringite crystallization in the C-S-H gel is believed to be the reason for expansion of the paste. This idea is further confirmed by Yang [10].

DEF not only occurs in preheated cementitious materials, but also in massive concrete structures [11, 12]. All concretes generate heat as cements hydrate. In thin items, the hydration heat dissipates almost as quickly as it is generated, while heat dissipates more slowly if it is generated in mass concrete. Therefore, the heat generated by the hydration of cement raises the temperature of concrete, leading to a significant temperature difference between the interior and the outside surface of the structures. The temperature induced by hydration in mass concrete may reach above 70 °C [12], which is high enough to induce DEF. If massive concrete structures are buried in a sulfate rich environment, for instance, in the saline soils and sea water which have a complex chemistry including magnesium, sulfate, sodium, chloride and dissolved $CO_2$ species [13], the coupling effect of ESA and DEF may occur.

ESA and DEF share some common aspects. The material mix has similar impact on ESA and DEF, for example, the high content of $C_3A$ and $C_3S$ contributes to the ettringite formation [14, 15]; a higher w/c ratio leads to a higher porosity and a higher permeability: on the one hand the latter leads to a faster ions transportation, such as $SO_4^{2-}$ ions from external solution under ESA condition, and on the other hand the former eases ettringite accommodation. Moreover, the most common degradation observation of cement-based materials are expansion and cracking. In both situations, the expansion is attributed to the formation of ettringite [16], though the gypsum is considered as the reason of ESA by some authors [17, 18, 19]. However, this hypothesis was not confirmed by the observation of gypsum precipitation after the cracks occur [18, 20].

Furthermore, several hypotheses were proposed to explain the expansion resulting from ettringite formation, including the volume increase theory [21],

colloidal expansion theory [22, 23], topochemical reaction theory [24], and the crystallization pressure theory [2, 3, 25] which is more recent and popular. With these similarities, a global expansion mechanism is investigated to explain the behavior of specimens under different sulfate attack conditions.

In this paper, with the aim of understanding the expansion mechanism, an experimental study on cement pastes exposed to three different sulfate attack conditions (ESA, DEF, and Coup) will be conducted, including the length and mass measurements, and the variation of PSD before and after sulfate attacks.

## 2. Materials, casting and curing

A cement CEM I 52.5 R CE CP2 NF [26] was used, the chemical compositions of which is presented in [27]. Six sets of small cement paste prisms ($2 \times 2 \times 12$ cm$^3$) and one set of big cement paste prisms ($11 \times 11 \times 22$ cm$^3$) were fabricated, with a water to cement ratio of 0.55, as shown in Table 1. The $2 \times 2 \times 12$ cm$^3$ prisms were subjected to three different sulfate attack conditions (ESA, DEF and the coupling effect of both reactions) and were tested at two states, initial and final states. The initial state is defined as the moment after the 28 days curing, right before exposing the specimens to their respective aging conditions. The final state for the specimens exposed to ESA and ESA+DEF is the time when the specimens are seriously degraded and show an expansion of around 1%. Different to ESA and Coup, the sigmoid expansion curve is the most typical kind in DEF, which includes a latent period, an accelerated increasing phase and a plateau part. The final state for DEF is the plateau phase. The $11 \times 11 \times 22$ cm$^3$ prism samples were designed to be subjected only to DEF, and were fabricated to characterize the pore size distribution (PSD) at different states: the initial state (after the 28-day curing), the latent period, and two different final states. The former two specimens were fabricated with slightly different fabrication procedures compared to two final specimens. Indeed, specimens designed to be tested at initial and latent period were cast with a specific mortar mixer while two final specimens were cast with a 30-liters concrete mixer;

moreover, for each set of specimens, a different mixing procedure was followed. The samples are named by type of exposure condition (ESA, DEF, and Coup for the coupled sulfate attack), the expansion state of the specimen (Initial, latent, and final state), and geometry (Table 1).

Table 1: Design of the samples.

| Specimens | Size ($cm^3$) | Expansion state |
|---|---|---|
| ESA-Ini | $2 \times 2 \times 12$ | Initial |
| ESA-Fin | | Final |
| DEF-Ini | | Initial |
| DEF-Fin | | Final |
| Coup-Ini | | Initial |
| Coup-Fin | | Final |
| DEF-Ini | $11 \times 11 \times 22$ | Initial |
| DEF-Lat | | Latent - expansion of 0.03% |
| DEF-Fin1 | | Plateau - expansion of 1.49% |
| DEF-Fin2 | | Plateau - expansion of 1.22% |

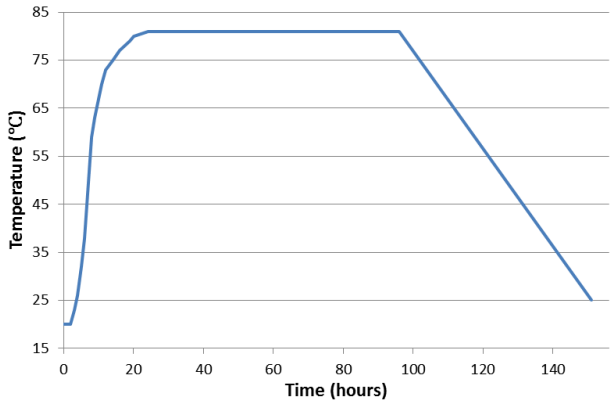


Figure 1: Heating treatment for samples subjected to DEF and Coup.

All the specimens were protected during their moist cure with a curing textile on the top surfaces after casting to prevent excessive leaching. For the specimens

dedicated to the DEF and the coupling effect tests, a heat treatment (Fig. 1) was applied in a tank containing water, with the temperature controlled by the heating device and following the same preheating procedure adopted in [7, 28]. The total duration of the heating process was 1 week. After casting, the formwork with the specimens was set aside for 2h (pre-curing time), and then the heat treatment started. The first step was to increase the temperature to 81 °C after 24 hours with a maximum rate of about 10 °C/h. Then, a constant temperature of 81 °C followed and was kept for 72 h. The heat treatment was completed by a cooling phase. The cooling rate was fixed at -1 °C/h to avoid a cracking of the bulk induced by a thermal effect. In the end, the heating was stopped at 25 °C. The objective of this temperature profile was to be representative of the curing conditions in the core of a massive structure [7]. For the specimens dedicated to the ESA tests, an ambient temperature (around 20 °C) curing in tap water (to keep the same moist environment as DEF) was applied, with a water to solid ratio (volume of storage water / volume of specimens) of around 26.

One week after the casting, specimens were demolded, namely after the heating treatment for DEF and Coup specimens. Then, the large prisms were kept under aluminium sealing for 28 days to keep the moisture constant in the specimens for a continuous hydration and to limit the effect of leaching. The small prisms were stored in tap water with a water to solid ratio (volume of stored water / volume of specimens) of around 26 until the end of the curing period (28 days) due to a high probability of losing moisture in small-size specimens.

After the curing period, the ESA and Coup specimens were immersed in a sodium sulfate solution $Na_2SO_4$, with a concentration of 15g/L (the solution was renewed each week during the first month, and then every two weeks after), and the DEF specimens were kept in tap water without any renewal. To summarize, four types of curing and exposure conditions were used in this study, see Table 2.

Table 2: Curing and storage conditions for specimens

| Specimens | Curing conditions | Storage conditions |
|---|---|---|
| ESA $2 \times 2 \times 12$ cm$^3$ | Water | $Na_2SO_4$ solution |
| DEF $2 \times 2 \times 12$ cm$^3$ | Heat treatment and subsequent in water | Water |
| Coup $2 \times 2 \times 12$ cm$^3$ | Heat treatment and subsequent in water | $Na_2SO_4$ solution |
| DEF $11 \times 11 \times 22$ cm$^3$ | Heat treatment and subsequent in aluminium sealing | Water |

## 3. Experimental techniques

### *3.1. Mass and length monitoring*

#### *3.1.1. Instrumentation and slicing of specimens*

All the specimens subjected to sulfate attacks were mass and length measured during degradation. In order to ensure the monitoring of the axial dimension, specimens were equipped with stainless steel pins after demolding (1 week after casting) on surfaces. Only three faces (see Fig. 2) were equipped with stainless steel pins, because the fourth face (the non-formed face) was not smooth enough due to the curing textile (shown in Fig. 3 (b)).

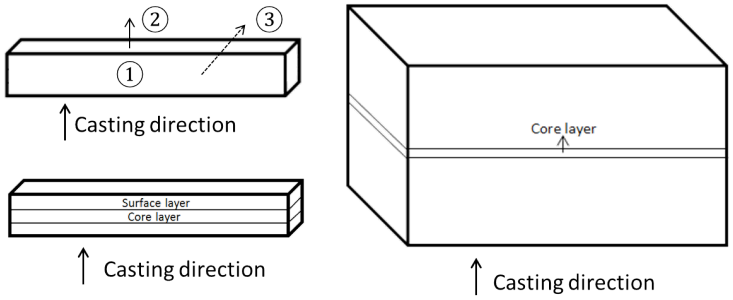


Figure 2: Slicing scheme for specimens


Figure 3: Instrumentation of the specimens

When the specimens were ready for the characterization of PSD, they were wet sawed, sliced, and prepared to be lyophilized (to remove the moisture and stop the hydration). As shown in Fig. 2, the small specimens were sliced from the top surface to bottom, and only the top two layers were selected. In order to limit the effect of leaching, since specimens were stored in a moist environment, which is most serious on the surface layer, the big specimens were studied only on the core layer (with a depth of 4.95-5.50 cm), see Fig. 2.

*3.1.2. Data post-processing*

The measured strain illustrates that the strain on the top face (face 2 in Fig. 2) is quite different compared to the other two side faces, especially in the case of ESA, see Fig. 4. The reason will be explained in the following section 4.3.2. Therefore, for $2 \times 2 \times 12$ cm$^3$ specimens, the expansion value on top face is not considered when calculating the average expansion of specimens (in other words, the expansion curves presented hereafter correspond to the mean value of expansion of faces 1 and 3); indeed, since the strain measurement on the fourth face is not available, there is no balance of the singular measurement of face 2. However, the big prisms had pins on four surfaces (their bigger dimensions allowed a better surface preparation to glue the pins), and the mean value of all 4 faces is presented.

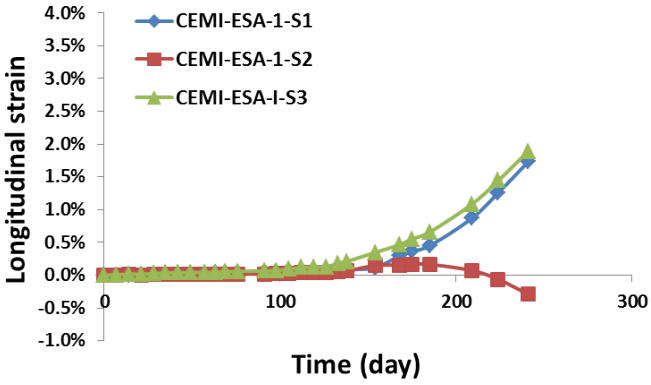


Figure 4: Strain of ESA $2 \times 2 \times 12$ cm$^3$ specimens on each measured face.

### *3.2. Mercury Intrusion Porosimetry – MIP*

The instrument used in this study is a Micromeritics' AutoPore IV 9500 series Porosimeter that is capable of exerting a maximum pressure of up to 414 MPa. The pore size range that could be investigated is between 3.7 nm and 400 $\mu$m. For each MIP test, about 1.0 g sample after lyophilization was selected. The low-pressure intrusion was performed first, followed by a high-pressure intrusion. All the pores are assumed to be fully accessible for mercury penetration from the surface of the specimen. However, in reality, the pores consist of large pores connected by smaller throats. This technique measures the largest entrance towards a pore, but not the actual inner size of a pore. Obviously, it can not be used to analyze closed pores either, since the mercury has no way of entering.

Although MIP has several limitations, the pore structures determined by this technique have been related to the factors that control the characterization of materials [29], such as total porosity, and PSD. Furthermore, MIP may be closer to the actual values than the other techniques even if mercury pressures can collapse the small pores or break through to the isolated pores [30]. MIP is useful in comparative studies of similar materials [31]; for example, this technique is found to illustrate the same shift in pore sizes as compared to image

analyses [32]. The characterization and the comparison of the PSD is one of the main objectives of the present study, which means that MIP is an appropriate technique. The MIP technique has practical limits and the measurement of the real pore geometry suffers distortion since this method measures actually the pore entry radius. However, this technique is precise and reproducible as a qualitative analysis method. It showed a relative variability of porosity measurements of 2% on two sets of samples (each conducted three times) [33]. The maximum relative difference between the highest and lowest total porosity for a given cement paste was 4% with an average standard error of 0.6% in [34], based on the measurement of 30 sets of specimens. The measured PSD curves showed good consistency as well. As a conclusion, distortion inherent to the MIP technique was assumed to affect the initial and damaged microstructure in the same way, so that a comparison between the state of microstructure during the degradation process is made possible.

## 4. Results and discussions

### *4.1. Observations*

The specimens were monitored during the different sulfate attacks. Fig. 5 illustrates a visual monitoring conducted on the specimens. First, in the case of ESA, a slight crack appeared at the bottom surface after only two months of contact with the sodium sulfate solution, and this crack extended to the side faces later. After around 7 months of testing, the specimens were so damaged that they even could break when measuring the length variations. At that moment, it was supposed that the cement pastes had lost all cohesion and that the damage was total. Furthermore, the bending of the specimen started with the appearance of cracks. This suggested that significant tensile stress was the cause of this degradation.

During the monitoring of the DEF specimens, a rancid odor similar to the smell of sulfur was first detected when the specimens were removed from the bath. Then, cracks were observed, but their appearance was much delayed in

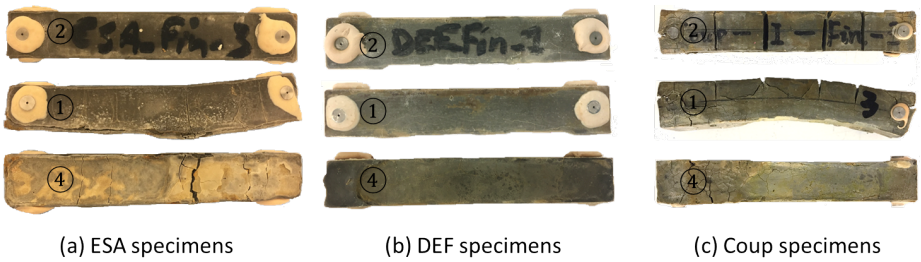


Figure 5: Observations of (a) ESA specimens after 7 months; (b) DEF specimens after 2 years; and (c) Coup specimens after 2.5 months on faces 1, 2 and 4.

time, with a lower degree of deterioration compared to ESA. After an immersion in water for up to 2 years, the monitoring of the DEF specimen was stopped due to the limited time of the experiment. The DEF specimens had an expansion around 0.5%, with slight cracks on the top and side surfaces. Finally, some whitish powdery material was observed coated on the surfaces of the specimens (not shown in the figure). The occurrence of the powder may be induced by leaching of lime compounds, which leads to the formation of calcium carbonate or calcium sulfate on the surface of the specimens. It may also be caused by sulfate efflorescence. A similar observation was found in the case of ESA with thaumasite formation [35], and the component of the powder was analyzed as either calcium and potassium sulfates or thenardite ($Na_2SO_4$).

For specimens exposed to the coupling effect of ESA and DEF, the time interval of degradation was short and the kinetic of swelling was fast compared to cases where ESA and DEF act separately. The first cracking appeared after approximately 1 month on the top surface. After an immersion in a sulfate solution during 2.5 months, the cement paste was totally damaged and the top surface of the specimens was separated into several sections because of the cracks. At the end of the monitoring, crystals could be clearly seen in the material, especially in the cracks. Apart from ettringite, this crystal formed in the cracks may also be gypsum [2]. From observations, specimens subjected to the coupling effect of ESA and DEF showed a more aggressive degradation.

*4.2. Length and mass variations*

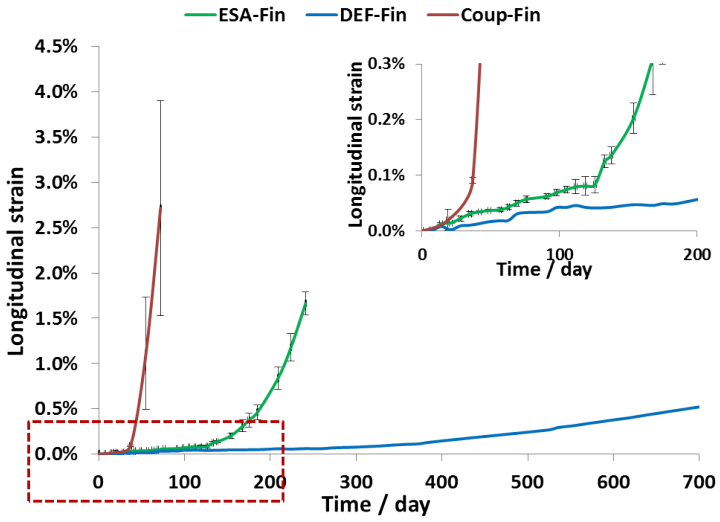


Figure 6: Length variations of the specimens exposed to ESA, DEF and Coupling.

Fig. 6 shows the average longitudinal strain of $2\times2\times12$ cm$^3$ specimens under different cases of sulfate attacks. In the case of ESA and Coup, they represent the average values of the three specimens belonging to the same set. The error bars correspond to plus/minus the standard deviation. For DEF, strain of one specimen is presented, due to the destructive measurements on the other two specimens during monitoring. The Coup specimens show a large standard deviation compared to the other ones, especially at high expansion level, which is the result of the variable response of materials to damage. Moreover, the high bending of the specimens, which happens at the late stage of degradation, induces errors in the measurement, the linear displacement between the stainless steel studs corresponding to only a part of the real deformation of the specimen. The coupling specimens show the highest expansion of around 2.7% after 2.5 months, and the DEF specimen shows the smallest expansion of 0.5%, which means that the specimen is in the accelerated stage. This order is consistent with the qualitative degree of cracking observed. These differences in kinetics

and amplitudes can originate from a greater source of $SO_4^{2-}$ for the coupling effect.

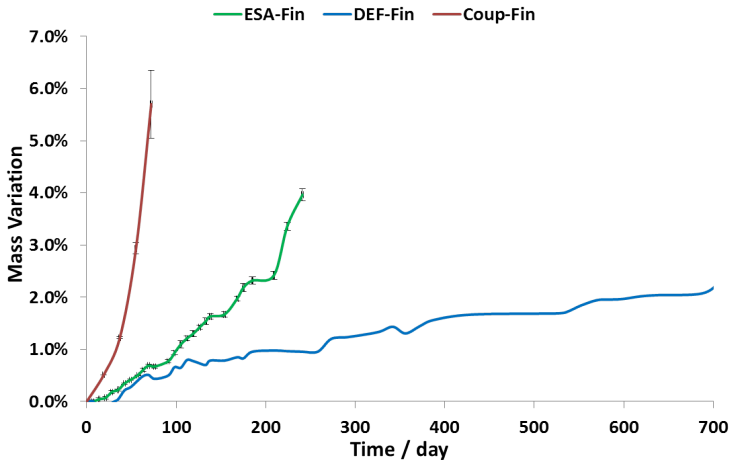


Figure 7: Mass variations of the specimens.

As shown in Fig. 7, the mass increases with time, and this could be explained by the penetration of $SO_4^{2-}$, forming ettringite for ESA and coupling specimens, in addition to water ingress happening for all attack cases considered in this work. The water penetrates in the pore solution on the one hand, and it interacts chemically to form new products on the other (e.g. a molecule of ettringite contains 32 water molecules).

The evolution of the strain as a function of the weight increase is presented in Fig. 8. It shows that the two variables are linked by a positive correlation. Below a strain threshold of 0.08%, the correlation showed a similar linear relationship with a slope of around 0.06 for three cases, when materials were in the elastic stage. However, in the following period, this relationship was affected by the type of sulfate attacks. DEF and ESA specimens followed the same route, and Coup specimens seem to be increased with a higher rate. As specimens are sensitive to the tensile stress during the damaged range, the content of the sulfate ions has a significant effect on the damage behavior of specimens.

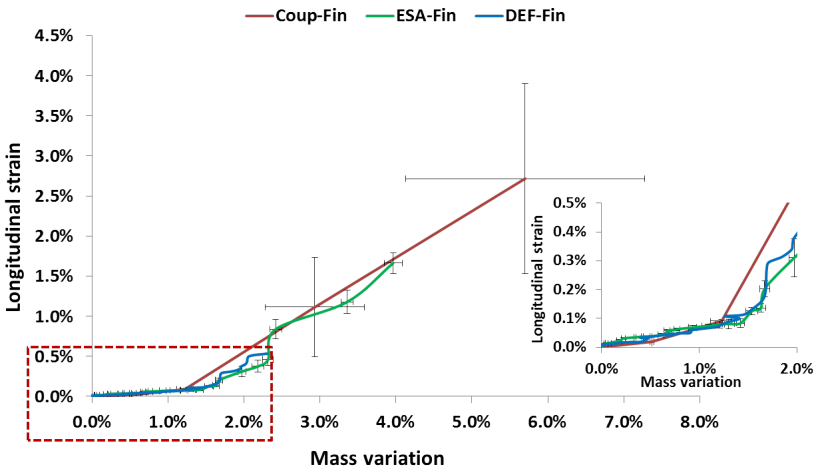


Figure 8: Evolution of the strain as a function of the weight gain.

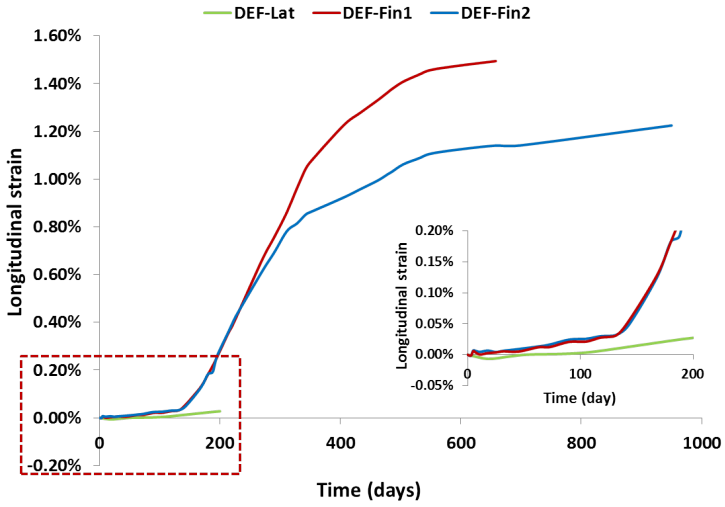


Figure 9: Strain of $11 \times 11 \times 22$ cm$^3$ specimens.

The longitudinal strain of the $11 \times 11 \times 22$ cm$^3$ DEF specimens is presented in Fig. 9. After a 200-day immersion in water, the specimen DEF-Lat shows an expansion of 0.03 %. The specimen DEF-Fin1 presents an expansion of 1.49% after 660 days, and DEF-Fin2 approaches to a swelling plateau of ap-

proximately 1.22% after 950 days. The latter two specimens showed a different swelling kinetic from DEF-Lat, which may be caused by slightly different casting procedures (see section 2) even though the materials and w/c were exactly the same. The slightly different fabrication procedures possibly led to different microstructures of the materials and resulted in a different response to the swelling.

### *4.3. Pore size distribution measured by MIP*

#### *4.3.1. Effect of possible processes on PSD*

In Portland cement, the main hydrate phases are portlandite and C-S-H. Portlandite may be present as thin elongated platelets of 10-100 nm in thickness [36, 37], and as large CH domains of high geometrical complexity of tens of micrometers in size [36, 38, 39], which highly depends on the curing conditions (air or wet) and hydration degrees [38]. The pores in hardened cement paste are divided into gel pores (less than 10 nm) and capillary pores (10 nm – several $\mu$m) [40]. The change of pore structure of cementitious materials due to leaching has been already studied. The effect of leaching on porosity is mainly on capillary pores with a range between 0.1-10 $\mu$m for one sample and 0.04-0.2 $\mu$m for another [41]. The pore volume increases due to the dissolution of CH has been found in [42]. The increased volume with a diameter of less than 100 nm is believed to be caused by the dissolution of C-S-H gel and that of pores larger than a few $\mu$m are due to the dissolution of CH. In [43], it was determined that, in dissolution tests of alite hydrate, the volume of pores with a size of around 1 $\mu$m increased along with the progress of the dissolution of the portlandite. Therefore, [43] assumed that pores of 0.2 $\mu$m or smaller were attributable mainly to the dissolution of C-S-H, while those larger than 0.2 $\mu$m were attributable mainly to the portlandite dissolution. While questioning the reliability of this classification, [43] asserted that there was a good correlation between the dissolution of portlandite and an increase in the volume of pores larger than 200 nm in leaching examinations of alite hydrate. However, [44] pointed out that the increase of pore volume in the range of 50 to 500 nm in

diameter can also be due to the dissolution of CH. The pore ranges derived from CH or C-S-H are not identified by scholars. However, the change in PSD caused by the dissolution of portlandite can be distinguished from the one in C-S-H. Therefore, it is assumed that the increase of pore volume with respect to pores between 10 nm and 1 $\mu$m is due to the dissolution of CH, and that the increase of pores with diameters less than 10 nm is related to the decalcification of C-S-H [41, 42, 43, 44].

In addition to the hydration process, the evolution of the PSD involves several processes, such as crystal formation, the dissolution of CH, the decalcification of C-S-H, and the growth of cracks. The resulting pore volume variation is thus determined by the kinetics/balance of these processes. For example, if the increased pore volume ($\delta V_1$) induced by cracks or hydrates dissolution is higher than the absolutely decreased one ($\delta V_2$) due to ettringite formation, the accumulated pore volume ($\delta V_1 - \delta V_2$) shows an increase, which means that the total pore volume in this range increases. Conversely, the pore volume in a given range decreases if ($\delta V_2$) is higher than ($\delta V_1$). This is an important point that will be taken into account when analyzing the variation of PSD in the following sections.

*4.3.2.* $2 \times 2 \times 12$ cm$^3$ *specimens*

Fig. 10(a) presents the PSD of the $2 \times 2 \times 12$ cm$^3$ specimens exposed to ESA. First of all, the initial sample shows similar pore characteristics at different layers, which indicates a homogeneous material after the curing. Then, this figure shows that the pore volume with entry diameters between 3.7 and 50 nm decreases after the ESA. The ettringite which leads to expansion was found to form in the pores less than 0.1 $\mu$m in the literature [2]. This results in a decrease of pore volume which is consistent with the results illustrated in figure 10. Therefore, it is supposed that the main generated crystal is ettringite [18, 20, 45] which forms in the gel and capillary pores during the ESA. The decrease of pore volume with entry diameters between 3.7 and 50 nm is observed in the surface layer, and a smaller decrease with respect to pores in the range

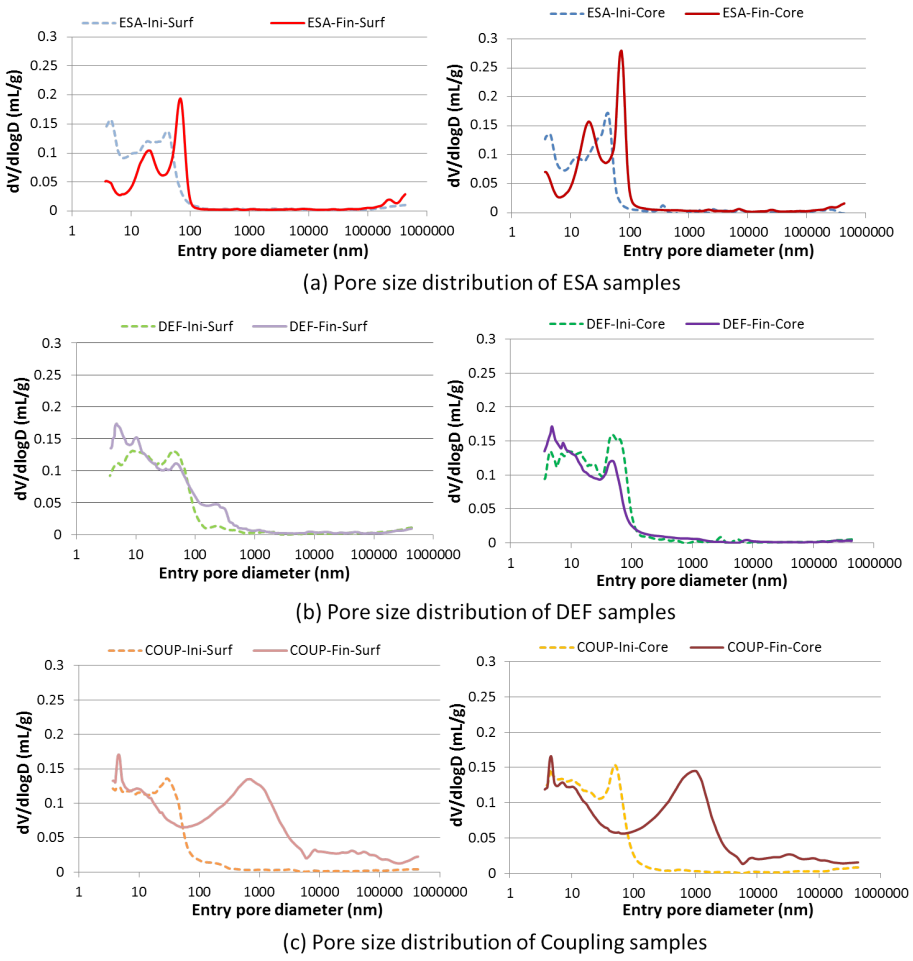


Figure 10: MIP-based PSD of $2 \times 2 \times 12$ cm$^3$ specimens submitted to (a) ESA; (b) DEF; and (c) Coupling.

of 3.7-13 nm and 27-51 nm at the core layer. It is due to the fact that more sulfate ions penetrated from the external solution and results in the formation of more ettringite in the surface layer. Almost all the AFm was transformed into ettringite at the surface layer, while the core layer was not sulfate attacked (specimen size $40 \times 40 \times 160$ mm$^3$) [2]. Furthermore, in the present work, an increase of pore volume at pores of approximately 100 nm is observed. On the

one hand, this can be explained by the dissolution of CH, which provides a high source of calcium during the ESA [46]. On the other hand, this is due to the formation of microcracks, the smallest size of which is around 0.1-0.25 $\mu$m [47]. The precipitation of ettringite in the capillary pores may lead to fractures in the portlandite phase, which is considered as the weakest part in hardened cement paste and responsible for the microcrack initiation and growth [48].

Fig. 10(b) presents the PSD of the $2\times2\times12$ cm$^3$ specimens exposed to DEF. First of all, the comparison of the initial PSD at different layers shows that the curves are similar but the core layer shows a higher pore volume at the range of 40-100 nm. The pore volume in this range corresponds to the spaces where hydration products (mainly CH) exist [49]. Thereby, the higher pore volume at the core layer may be attributed to a lower degree of hydration. Further, a decrease of pore volume in the pore range of 9.7-100 nm is found in the surface and core layers. It means that the pore volume filled by the generated crystals is larger than the one that may be created by the dissolution of CH. This indicates the formation of crystals in the pores between 9.7-100 nm. The crystals may form in smaller pores as well, while the corresponding decreased pore volume is balanced by the increased pore volume due to the decalcification of C-S-H for example. As ettringite is believed to be the reason for the expansion, then the precipitated crystal is supposed to be ettringite. However, the ettringite was postulated to initially precipitate in C-S-H gel corresponding to a pore size less than 10 nm and then in cracks and voids [5, 8, 9], which is not consistent with the results obtained in this study. The results presented in Fig. 10(b) come from a $2\times2\times12$ cm$^3$ DEF specimen which has an expansion of 0.5%. Consequently, a question remains: will ettringite continue to form in smaller pores when the expansion becomes higher? This question will be answered in the next section while analyzing the experimental results of $11\times11\times22$ cm$^3$ DEF specimens. An increase of pore volume between 3.7 and 9.7 nm is observed in this figure as well. This should be attributed to the decalcification of C-S-H, as demonstrated in section 4.3.1. In addition, the surface layer shows an increase of pore volume between 100 nm and 1 $\mu$m, which is due to the dissolution of

CH and to microcracks, as explained in the case of ESA.

Fig. 10(c) presents the PSD of $2 \times 2 \times 12$ cm$^3$ specimens exposed to coupling effect of ESA and DEF. The initial state of the material shows a similar PSD at different layers except for a pore range between 40 and 100 nm. The core layer shows a larger pore volume around 100 nm, which could be attributed to a smaller degree of hydration. From the comparison of PSD before and after degradation, it can be concluded that pore volume between 5.3 and 80 nm decreases. A huge space is released in pores with diameter larger than 80 nm. It is due to the dissolution of CH and the occurrence of microcracks, which is also seen in the pores of less than 5.3 nm induced by the decalcification of C-S-H. Compared to the other two cases, a much higher pore space is freed in the pores larger than 1 $\mu$m. This is related to the occurrence of cracks which results from a worst degradation. After the degradation, the coupling samples show a more homogeneous PSD at different layers, which is attributed to the high diffusion of ions [29] after a high degree of deteriorations.

The comparison of PSD of samples among different exposure conditions are presented in Fig. 11. First, in Fig. 11(a), the initial PSD of DEF and Coup specimens show a larger pore volume between 5-19 nm at the surface layer and between 5-22 nm at the core layer compared to ESA specimens. One reason is that the decomposition of primary ettringite during the preheating treatment [5, 6, 7] results in an increase of pore volume. Another reason is that the high temperature helps mineral ions (e.g. Al and Fe) to migrate from the reaction sites of anhydrous phases into the inner product in the C-S-H [50] chemically or physically, which further enhances the porosity in this range.

Table 3: Porosity of initial $2 \times 2 \times 12$ cm$^3$ at surface and core layers

| | ESA-Ini | DEF-Ini | Coup-Ini |
|---|---|---|---|
| Surface layer | 25.9% | 28.2% | 25.5% |
| Core layer | 23.4% | 29.6% | 26.4% |

In addition, the porosity of initial $2 \times 2 \times 12$ cm$^3$ specimens (after curing) at

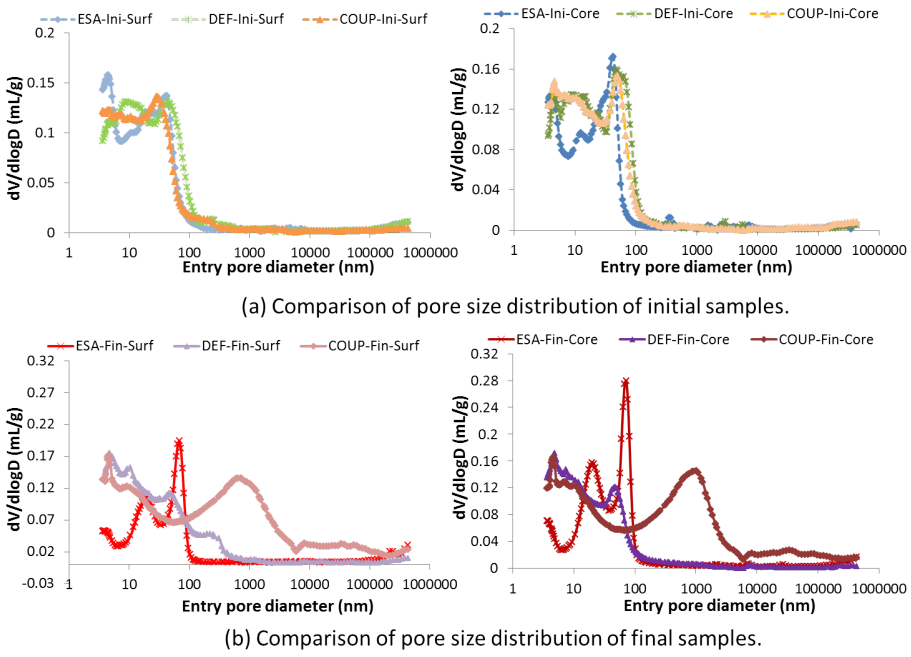


Figure 11: Comparison of PSD of samples from MIP.

the surface and core layers are summarized in Table 3. A porosity difference is found along the depths, even though in different trend whether the specimens were preheated or not. After the heating treatment, a lower porosity is observed at the surface layer (DEF-Ini), which was in contact with the bottom of the moulds during the heating treatment. A porosity gradient from the upper-water face to the lower face was reported in [51], which was explained to be due to the higher effective w/c ratio at the upper-water surface and the vertical vibration process. Conversely, ESA-Ini shows a higher porosity at the surface layer. A low porosity has a positive effect to resist sulfate attack from the aspects of low diffusion of aggressive ions from external solution and strong mechanical properties, and meanwhile a negative effect due to low space to accommodate expansive products. In this study, the low porosity presents a negative effect consistently in the case of Coupling effect and ESA. This explains the observed

bending of specimens (see section 4.1), and the different gradients of porosity in ESA and Coup lead to the downward and upward bending, respectively. However, the bending did not happen in the case of DEF, which is probably due to a limited expansion of 0.5%.

Secondly, the final PSD of specimens are affected by exposure conditions. In the pore range of 3.7-50 nm at the surface layer and between 3.7-20 nm at the core layer, ESA samples show more reduced pore volume than the other two cases, and the coupling samples show a similar PSD as DEF samples in these ranges, respectively. Although provided with more sulfate ions from the aggressive solution in the case of coupling effect, ettringite preferentially precipitates in the cracks that appeared soon after the immersion, which leads to a further degradation. A similar situation was found in the case of ESA, [52] found that the ettringite existed in cracks after being stored in the sodium sulfate solution. It appeared to have been deposited after the crack had been formed. In addition, this crystal formed in the cracks may also be gypsum [2].

The variations of the pore volume in different pore ranges at the core layer are summarized in Fig. 12. The pores are categorized according to the variation of pore volume after the attacks. First, the figure illustrates the pore range where the pore volume is decreased. For example, the decreased pore volume distributes between 3.7 and 50 nm for ESA-Core, and 9.7-100 nm in the case of DEF-Core. For Coup-Core, the occupied pores are between 5.3 and 80 nm. These pore ranges are consistently within the capillary and gel pores. Then, the figure illustrates increased pore volumes mainly above 80 nm, which are the results of the dissolution of portlandite and the occurrence of microcracks. Furthermore, the pore volume after degradation is predicted by adding the initial porosity (measured by MIP) to the pore volume of cracks, which is equal to 3 times the macroscopic measured expansion $\epsilon$ based on the assumption that expansion only leads to the formation of cracks. The predictions for ESA and DEF specimens show a higher value compared to the one measured by MIP, that can be explained by the fact that part of the generated cracks are filled with crystals. Moreover, a relatively lower prediction for Coup specimen may

be due to an underestimation of strain caused by bending.

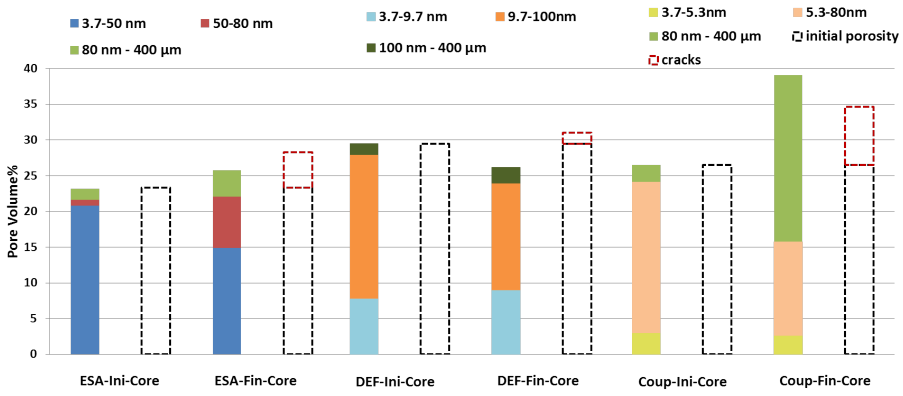


Figure 12: Pore volume variation of $2 \times 2 \times 12$ cm$^3$ specimens in the core layer (the pore volume of cracks is calculated as volumetric space, which is equal to 3 times the macroscopic measured expansion $\epsilon$).

A conclusion can be drawn according to the results of $2 \times 2 \times 12$ cm$^3$ specimens: **Ettringite is found to be formed in capillary and gel pores both in the case of ESA and Coup, while mainly in capillary pores for DEF with the limited expansion of 0.5% investigated in this study.** Then two questions can be raised for DEF: will the generated crystals continue to form in smaller pores if the expansion is higher than 0.5%? And how does the PSD evolve during sulfate attacks? These will be analysed in the following section.

### *4.3.3.* $11 \times 11 \times 22$ cm$^3$ *specimens*

The evolution of the PSD of the DEF samples in the core layer is presented in Fig. 13(a). This layer has been selected because of the limited effect of calcium leaching in the core of the $11 \times 11 \times 22$ cm$^3$ specimens. The comparison of the DEF-Ini-Core and DEF-Lat-Core (expansion of 0.03%) shows that pores between 100 nm and 1 $\mu$m are filled (thus, even if voids have been created in this range, the volume of ettringite formed was higher), while pores between 10 and 100 nm are released after a 200-day immersion in water (thus, even if crystals

have precipitated in this range, the volume of pores formed was higher). When the specimen DEF-Fin1 reaches an expansion degree of 1.49%, pores between 4 and 80 nm are occupied after the latent state, and pores larger than 80 nm are released. In parallel, when the specimen DEF-Fin2 reaches an expansion degree of 1.22%, pore volume between 3.7-20 nm and 45-75 nm is decreased after the latent state, and increased with pores larger than 75 nm. If specimen DEF-Fin2 is compared to DEF-Ini, the conclusion would be that after DEF, the pore volume of pores between 4-20 nm and 100 nm - 1 $\mu$m is decreased, while pore volume between 20-100 nm is increased. During DEF, the pore volume in pores between 4-20 nm tends to decrease while pore volume evolution with respect to pores larger than 20 nm is variable. The latter phenomenon depends on complicated processes, including the dissolution of CH, ettringite formation and the occurrence of cracks.

To easily and better understand the evolution of the pore structure of 11 $\times$ 11 $\times$ 22 cm$^3$ DEF specimens, the pores are categorized into different ranges: 3.7-20 nm, 20-100 nm, and 100 nm - 400 $\mu$m based on the variations of PSD which have been discussed above (Fig. 13(b)). First, compared to DEF-Ini-Core, DEF-Lat-Core shows an obvious decrease of pore volume in the range of 100 nm - 400 $\mu$m and an increase of pore volume in the range of 20-100 nm, with the total porosity decreasing from 31.9% to 28.0%. It could be explained by the fact that calcium released from the dissolution of CH and the decalcification of C-S-H in the range of 3.7-100 nm reacts with the available aluminium and sulfate ions to form ettringite, which forms in the range of 100 nm - 400 $\mu$m. However, the generated crystals in these voids do not lead to a major expansion based on the macroscopic expansion measurements. Then, a decrease of pore volume in the pores 3.7-20 nm, an increase of pore volume in the range of 100 nm - 400 $\mu$m, and a constant pore volume in the range of 20-100 nm are observed in the sample DEF-Fin1-Core. The constant pore volume in red part does not mean that no crystals are generated, but a balanced process occurs between the dissolution of CH and the precipitation of the generated crystals. In addition to a decrease of pore volume in blue part, it is concluded that the generated

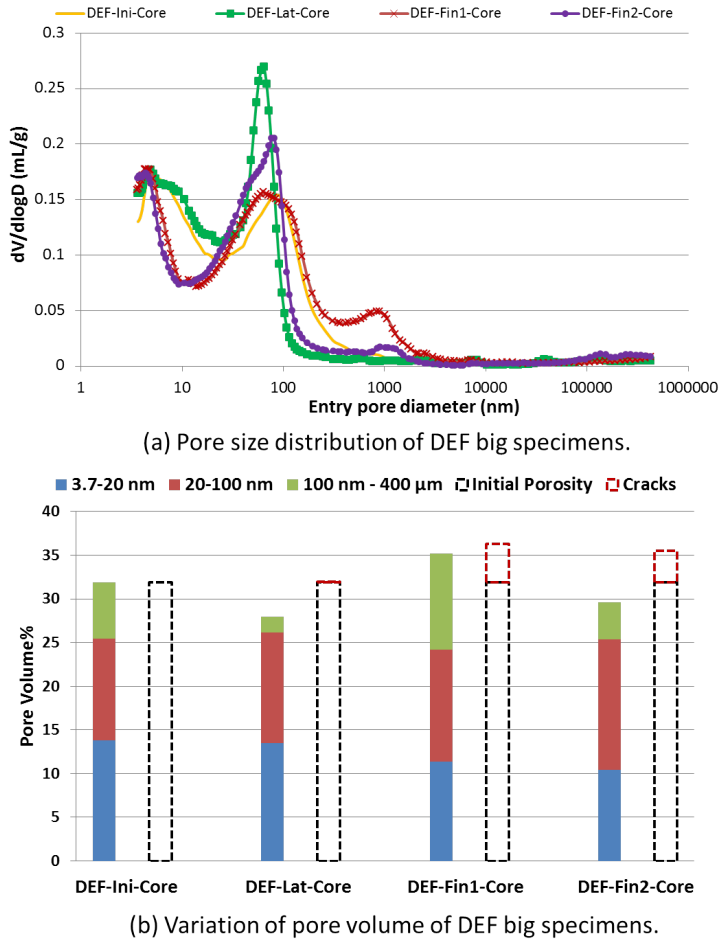


Figure 13: Pore size distribution (a) and pore volume variation (b) of DEF $11 \times 11 \times 22$ cm$^3$ specimens from MIP in the core layer.

crystal is penetrating through the pores between 100 nm - 400 $\mu$m into smaller pores compared to DEF-Lat-Core, which corresponds to expansion. A similar phenomenon of decrease in blue part can be observed for specimen DEF-Fin2-Core, while in the red part, the pore volume released by the dissolution of CH is higher than the one occupied by generated crystals. Among these generated crystals, some may form without generating any expansion. Even though it is

difficult to separate the expansive crystals from the harmless ones, it is sure that at least part of the generated crystals are the reason for expansion. Moreover, the increased pore volume with respect to pores between 100 nm - 400 $\mu$m could be attributed to the dissolution of CH and the occurrence of microcracks. In addition, the generated crystals may precipitate in these pores as well, but with a weak ability to stop the pore volume increasing. The difference on expansion degree between these two final specimens may come from the different total porosity (35.2% for DEF-Fin1 and 29.6% for DEF-Fin2), if the initial porosity is assumed to be the same. To be more specific, a relatively lower occupation of generated crystals in the pores between 20-100 nm leads to less expansion in DEF-Fin2-Core, which shows a lower pore volume in the pore range of 100 nm - 400 $\mu$m. This further confirms that crystal precipitation in the capillary and gel pores is the reason for expansion, and results in cracks in the pores between 100 nm - 400 $\mu$m.

A damage mechanism can be suggested from the above analyses. **The generated crystals form in the biggest pores without generating an obvious expansion during the latent period, and then penetrate into smaller capillary and gel pores from which the expansion starts to increase rapidly.** The crystallization through macro to nano pores can be explained by the fact that large crystals are more energetically favored than small ones [53]. As discussed at the beginning of this section, it could not be determined neither the generated crystals are ettringite or all the generated crystals lead to an expansion. Nevertheless, based on the studies in the literature, it can be qualitatively concluded that the generated crystals have a high possibility to be ettringite, then the formation of ettringite in the capillary and gel pores is the reason for expansion.

## 5. Conclusions and discussions

Specimens exposed to ESA, DEF and the coupling effect of both were monitored during the degradation process. The greatest degree of degradation has

been found with coupling specimens, while the DEF specimen shows the smallest degree after around 700 days of monitoring (DEF degradations were however not finished). This order is consistent with the length variations. At the beginning stage, the increase of length shows a unique linear relationship with the increase of mass whatever the exposure conditions.

The variations of the PSD were measured by MIP. It is assumed that expansion is due to precipitation of crystals which are assumed to be ettringite. By analyzing the PSD change of $2 \times 2 \times 12$ cm$^3$ specimens subjected to ESA and Coupling effect, it is concluded that ettringite forms both in the capillary and gel pores. For the $2 \times 2 \times 12$ cm$^3$ specimens subjected to DEF, the presence of ettringite is confirmed mainly in the capillary pores with a limited expansion of 0.5%. Meanwhile, the ettringite tends to precipitate in the newly generated large voids, for example, microcracks. It further confirms that the ettringite formed in the cracks is not the reason for the expansion [1], but that it could nonetheless lead to a greater level of degradation where it already happened.

Then the PSD of the $11 \times 11 \times 22$ cm$^3$ DEF specimens confirm that the ettringite forms in smaller gel pores when the expansion increases from 0.5% to more than 1.0%. Moreover, a modification of the PSD during the attack is observed and a damage mechanism is proposed: the generated crystals tend to precipitate in the big pores without inducing obvious expansion, and then penetrate into capillary and gel pores, which leads to swelling.

The measured results of PSD variations presented above indeed include a combination of several phenomena, for instance, the dissolution of CH, the decalcification of C-S-H, and ettringite formation. Hence, the measured pore volume in a pore range cannot distinguish the different phenomena. However, this method provides a way to qualitatively understand the variation of the microstructure of specimens during the sulfate attack process.

In order to better understand the variation of the pore structure, it would be interesting to extend this study with chemical analyses, in particular to distinguish the effect of calcium leaching and crystals precipitation on the variation of pore volume. This would provide a quantitative analysis, which would allow a

better understanding of the consequences of each process. Additionally, extending the current study on cement paste to studies on mortar and concrete will be interesting and useful, which could be applied in the industrial engineering field.

## References


[1] M. Santhanam, M. Cohen, J. Olek, Mechanism of sulfate attack: a fresh look: part 1: summary of experimental results, Cement and Concrete Research 32 (6) (2002) 915–921. doi:10.1016/S0008-8846(02)00724-X.

[2] C. Yu, W. Sun, K. Scrivener, Mechanism of expansion of mortars immersed in sodium sulfate solutions, Cement and Concrete Research 43 (2013) 105–111. doi:10.1016/j.cemconres.2012.10.001.

[3] X. Ping, J. Beaudoin, Mechanism of sulphate expansion i. thermodynamic principle of crystallization pressure, Cement and Concrete Research 22 (4) (1992) 631–640. doi:10.1016/0008-8846(92)90015-N.

[4] A. Chabrelie, Mechanisms of degradation of concrete by external sulfate ions under laboratory and field conditions, EPFL.

[5] H. Taylor, C. Famy, K. Scrivener, Delayed ettringite formation, Cement and Concrete Research 31 (5) (2001) 683–693. doi:10.1016/S0008-8846(01)00466-5.

[6] N. Baghdadi, J. Seignol, R. Martin, J. Renaud, F. Toutlemonde, Effect of early age thermal history on the expansion due to delayed ettringite formation: experimental study and model calibration, in: Euro Mediterranean symposium on Advances in Geomaterials AGS'08, 2008, pp. 661–666.

[7] R. Martin, Analyse sur structures modèles des effets mécaniques de la réaction sulfatique interne du béton, Ph.D. thesis, Université Paris-Est (2010).

[8] M. Lewis, Heat curing and delayed ettringite formation in concretes, Ph.D. thesis, Imperial College London (University of London) (1996).

[9] M. Lewis, K. Scrivener, S. Kelham, Heat curing and delayed ettringite formation, MRS Online Proceedings Library Archive 370. doi:10.1557/PROC-370-67.

[10] R. Yang, C. Lawrence, C. Lynsdale, J. Sharp, Delayed ettringite formation in heat-cured portland cement mortars, Cement and Concrete Research 29 (1) (1999) 17–25. doi:10.1016/S0008-8846(98)00168-9.

[11] D. Hobbs, Expansion and cracking of concrete attributed to delayed ettringite formation, Proceedings of a 'technical Session–Ettringite: The sometimes host of destruction, American Concrete Institute, Seattle, Washington, SP-177 (1999) 151–181.

[12] L. Divet, A. Pavoine, Delayed ettringite formation in massive concrete structures: an account of some studies of degraded bridges, in: International RILEM Workshop on Internal Sulfate Attack and Delayed Ettringite Formation, RILEM Publications SARL, 2004, pp. 98–126.

[13] D. Kester, R. Pytkowicx, Sodium, magnesium, and calcium sulfate ion-pairs in seawater at 25c, Limnology and Oceanography 14 (5) (1969) 686–692. doi:10.4319/lo.1969.14.5.0686.

[14] C. Ouyang, A. Nanni, W. Chang, Internal and external sources of sulfate ions in portland cement mortar: two types of chemical attack, Cement and Concrete Research 18 (5) (1988) 699–709. doi:10.1016/0008-8846(88)90092-0.

[15] S. Al-Dulaijan, M. Maslehuddin, M. Al-Zahrani, A. Sharif, M. Shameem, M. Ibrahim, Sulfate resistance of plain and blended cements exposed to varying concentrations of sodium sulfate, Cement and Concrete Composites 25 (4) (2003) 429–437. doi:10.1016/S0958-9465(02)00083-5.

[16] R. Gollop, H. Taylor, Microstructural and microanalytical studies of sulfate attack iii. sulfate-resisting portland cement: Reactions with sodium and magnesium sulfate solutions, Cement and Concrete Research 25 (7) (1995) 1581–1590. doi:10.1016/0008-8846(95)00151-2.

[17] P. Mehta, Sulfate attack on concrete–a critical review, Material Science Concrete, IIIpp. 105 (1992) .

[18] T. Schmidt, B. Lothenbach, M. Romer, J. Neuenschwander, K. Scrivener, Physical and microstructural aspects of sulfate attack on ordinary and limestone blended portland cements, Cement and Concrete Research 39 (12) (2009) 1111–1121. doi:10.1016/j.cemconres.2009.08.005.

[19] J. Marchand, E. Samson, Y. Maltais, J. Beaudoin, Theoretical analysis of the effect of weak sodium sulfate solutions on the durability of concrete, Cement and Concrete Composites 24 (3) (2002) 317–329. doi:10.1016/S0958-9465(01)00083-X.

[20] E. Irassar, V. Bonavetti, M. Gonzalez, Microstructural study of sulfate attack on ordinary and limestone portland cements at ambient temperature, Cement and Concrete Research 33 (1) (2003) 31–41. doi:10.1016/S0008-8846(02)00914-6.

[21] B. Sheetz, S. Kwan, Control of ettringite swelling, Ashlines 4 (1) (2003) 1–10.

[22] Y. Fu, Delayed ettringite formation in Portland cement products, University of Ottawa (Canada), 1996. doi:10.20381/ruor-7976.

[23] P. Mehta, Mechanism of expansion associated with ettringite formation, Cement and Concrete Research 3 (1) (1973) 1–6. doi:10.1016/0008-8846(73)90056-2.

[24] M. Cohen, Modeling of expansive cements, Cement and Concrete Research 13 (4) (1983) 519–528. doi:10.1016/0008-8846(83)90011-X.

[25] R. Flatt, G. Scherer, Thermodynamics of crystallization stresses in def, Cement and Concrete Research 38 (3) (2008) 325–336. doi:10.1016/j.cemconres.2007.10.002.

[26] EN, 197-1: 2011, Cement, Composition, Specifications and Conformity Criteria for Common Cements.

[27] Y. GU, Experimental pore scale analysis and mechanical modeling of cement-based materials submitted to delayed ettringite formation and external sulfate attacks, Ph.D. thesis, Université Paris Est, Marne-la-Vallée, France (2018).

[28] R. Martin, F. Toutlemonde, Theoretical and experimental validation of a simple method to reproduce representative def-prone conditions in laboratory, Materials and Structures 46 (8) (2013) 1245–1255. doi:10.1617/s11527-012-9967-2.

[29] D. Roy, Relationships between permeability, porosity, diffusion and microstructure of cement pastes, mortar, and concrete at different temperatures, MRS Online Proceedings Library Archive 137. doi:10.1557/PROC-137-179.

[30] J. Beaudoin, Porosity measurement of some hydrated cementitious systems by high pressure mercury intrusion-microstructural limitations, Cement and Concrete Research 9 (6) (1979) 771–781. doi:10.1016/0008-8846(79)90073-5.

[31] H. Giesche, Mercury porosimetry: a general (practical) overview, Particle & particle systems characterization 23 (1) (2006) 9–19. doi:10.1002/ppsc.200601009.

[32] S. Diamond, M. Leeman, Pore size distributions in hardened cement paste by sem image analysis, MRS Online Proceedings Library Archive 370. doi:10.1557/PROC-370-217.

[33] R. Ragoug, O. Metalssi, F. Barberon, J. Torrenti, N. Roussel, L. Divet, J. de Lacaillerie, Durability of cement pastes exposed to external sulfate attack and leaching: Physical and chemical aspects, Cement and Concrete Research 116 (2019) 134–145. doi:10.1016/j.cemconres.2018.11.006.

[34] R. Cook, K. Hover, Mercury porosimetry of hardened cement pastes, Cement and Concrete Research 29 (6) (1999) 933–943. doi:10.1016/S0008-8846(99)00083-6.

[35] S. Chinchón Payá, A. Aguado de Cea, H. Nugteren, S. Chinchón Yepes, External sulfate attack in dam concretes with thaumasite formation, Materiales de Construcción 65 (317) (2015) 042. doi:10.3989/mc.2015.10513.

[36] P. Stutzman, Materials science of concrete special volume: Calcium hydroxide in concrete, Proceedings-Anna Maria Island-FL (2000) 59.

[37] G. Groves, Microcrystalline calcium hydroxide in portland cement pastes of low water/cement ratio, Cement and Concrete Research 11 (5-6) (1981) 713–718. doi:10.1016/0008-8846(81)90029-6.

[38] N. Hernandez, J. Lizarazo-Marriaga, M. Rivas, Petrographic characterization of portlandite crystal sizes in cement pastes affected by different hydration environments, Construction and Building Materials 182 (2018) 541–549. doi:10.1016/j.conbuildmat.2018.06.142.

[39] W. French, Concrete petrography: a review, Quarterly Journal of Engineering Geology and Hydrogeology 24 (1) (1991) 17–48. doi:10.1144/GSL.QJEG.1991.024.01.03.

[40] P. Monteiro, Concrete: microstructure, properties, and materials, 2006.

[41] T. Van Gerven, G. Cornelis, E. Vandoren, C. Vandecasteele, Effects of carbonation and leaching on porosity in cement-bound waste, Waste Management 27 (7) (2007) 977–985. doi:10.1016/j.wasman.2006.05.008.

[42] K. Haga, S. Sutou, M. Hironaga, S. Tanaka, S. Nagasaki, Effects of porosity on leaching of ca from hardened ordinary portland cement paste, Cement and Concrete Research 35 (9) (2005) 1764–1775. doi:10.1016/j.cemconres.2004.06.034.

[43] K. Haga, S. Sutou, M. Toyohara, M. Kaneko, Y. Kobayashi, T. Kozawa, Alteration of cement hydrate by dissolution, 1. alternation test of hydrate cement paste by water-permeation using centrifugal force, Nippon Genshiryoku Gakkai Wabun Ronbunshi 1 (1) (2002) 20–29.

[44] H. Saito, A. Deguchi, Leaching tests on different mortars using accelerated electrochemical method, Cement and Concrete Research 30 (11) (2000) 1815–1825. doi:10.1016/S0008-8846(00)00377-X.

[45] S. Yang, X. Zhongzi, T. Mingshu, B. Mather, Discussion of the process of sulfate attack on cement mortars, Advanced Cement Based Materials 5 (3-4) (1997) 109–110.

[46] R. Gollop, H. Taylor, Microstructural and microanalytical studies of sulfate attack. i. ordinary portland cement paste, Cement and Concrete Research 22 (6) (1992) 1027–1038.

[47] S. Diamond, Microstructure of cement-based systems/Bonding and interfaces in cementitious materials, 2002.

[48] Z. Yan-Rong, K. Xiang-Ming, L. Zi-Chen, L. Zhen-Bao, Z. Qing, D. Bi-Qin, X. Feng, Influence of triethanolamine on the hydration product of portlandite in cement paste and the mechanism, Cement and Concrete Research 87 (2016) 64–76. doi:10.1016/j.cemconres.2016.05.009.

[49] A. Muller, Characterization of porosity & csh in cement pastes by 1h nmr, Faculté des Sciences et Techniques de l'Ingénieur (2014) .doi:10.5075/epfl-thesis-6339.

[50] K. Kjellsen, Heat curing and post-heat curing regimes of high-performance concrete: influence on microstructure and csh composition, Cement and

Concrete Research 26 (2) (1996) 295–307. doi:10.1016/0008-8846(95)00202-2.

[51] B. Kchakech, Étude de l'influence de l'échauffement subi par un béton sur le risque d'expansions associées à la réaction sulfatique interne, Ph.D. thesis, Université Paris-Est (2015).

[52] J. Nielsen, Investigation of resistance of cement paste to sulfate attack, Highway Research Record (1966) 113.

[53] A. Adamson, A. Gast, Physical chemistry of surfaces 150 (1967) .